

Reconfigurable plasmonic hot spots enabled by composite VO₂–gold plasmonic antennas

Rostislav Řepa,^{1,2,*} Jiří Kabát,^{1,2} Tomáš Šíkola,^{1,2} and Vlastimil Křápek^{1,2,†}

¹Brno University of Technology, Central European Institute of Technology, Purkyňova 123, 612 00 Brno, Czechia

²Brno University of Technology, Institute of Physical Engineering, Technická 2, 616 69 Brno, Czechia

(Dated: March 13, 2026)

We theoretically investigate the formation of electric and magnetic hot spots with reconfigurable plasmonic antennas. We consider three material systems offering different levels of reconfigurability: gold with the static response, vanadium dioxide which allows for ON/OFF switching, and composite gold–vanadium dioxide material platform which offers a possibility to switch between the electric and magnetic hot spot within a single antenna. Using bowtie and diablo antennas as a case study, we evaluate optical response functions (scattering and absorption cross-sections, electric and magnetic field enhancement). We demonstrate that the composite material system brings, in addition to enhanced reconfigurability, also novel features of plasmonic antennas, such as strong optical absorption and a joint electric-magnetic hotspot.

Introduction Plasmonic antennas [1] (PAs) enable nanoscale control of light by means of the excitation of localized surface plasmons (LSPs). One of their most desired functionality is the formation of hot spots: deeply subwavelength volumes in which the electromagnetic field supported by PAs is particularly strong. When an object is inserted into the hot spot of a PA, its interaction with the light is significantly enhanced. Enhancement factors for the electric component of the field as large as 10^2 – 10^3 are being commonly reported [2–4]. Consequently, hot spots are exploited in numerous applications that rely on strong light-matter interactions. They include sensing [5], catalysis [6, 7], surface enhanced Raman spectroscopy [8], plasmon enhanced photoluminescence [9], plasmon enhanced electron paramagnetic resonance [10], strong plasmon-exciton coupling [11], optical trapping [12], or local heat management [13].

The most common PA designs supporting hot spots are a gap between two parts of a dimer PA [3] or a sharp tip or edge of a monolithic PA [14], with advanced concepts including the exploitation of Babinet’s principle in the dimer plasmonic apertures [15, 16] or hierarchical plasmonic nanostructures [17] also being developed. It is noteworthy that the enhancement of the electric and magnetic fields is often not equally strong. Based on the dominant component, the hot spots can be classified as electric (most frequent, with the majority of the previous references related to them), magnetic (also frequent [10, 15, 18]), or mixed (those with a balanced enhancement of both fields are rather rare [19, 20]). Bowtie and diablo PAs [15, 21] [Fig. 1(a)] are particularly attractive for the formation of electric and magnetic hot spots, respectively. Their shape similarity (they both consist of triangular metallic wings which are coupled capacitively in the case of the bowtie and conductively in the case of the diablo) has been recognized [15, 20] and led to a proposal of a reconfigurable PA which can be switched between the bowtie and the diablo functionality [20].

PAs composed of conventional metals have their functionality fixed after their fabrication. Driven by the desire for reconfigurable and tunable PAs, exploitation of phase-change materials (PCMs) is being considered. Vanadium dioxide (VO₂) represents one of the most popular PCMs for plasmonic applications. It exhibits a metal-insulator transition (MIT) with a convenient transition temperature around 68 °C, which can be triggered by thermal, electrical, mechanical, or optical stimuli [22]. During the MIT, the material exhibits significant changes in electrical conductivity (five orders of magnitude within a picosecond timescale) and optical properties (especially in the infrared region) [22, 23]. However, VO₂ also possesses some unfavourable properties, such as low optical conductivity even in the metallic phase and low Q factor of plasmon resonances [24], as well as restricted functionality, often limited to ON/OFF switching [25].

In our paper, we inspect the possibility to realize reconfigurable plasmonic hot spots using VO₂. To overcome its unfavourable properties, we propose to combine VO₂ as the active element and a conventional metal (gold) as a good conductor into composite PAs using a planar arrangement of both materials. Specifically, we focus on the bowtie and diablo PAs with the gold wings and VO₂ bridge [Fig. 1(a)], where switching between the bowtie and the diablo functionality shall be achieved by switching VO₂ between the insulating and the conducting phases. To assess the performance of the proposed composite material platform, we also inspect homogeneous bowtie and diablo PAs made of either gold or VO₂. We demonstrate that the composite PAs support hot spots with unique properties (balanced electric and magnetic enhancement), exhibit extensive tunability (in terms of the resonant energy and scattering and absorption efficiencies, but not so much in terms of the electric and magnetic enhancement), and outperform pure VO₂ PAs in terms of the magnitude of the enhancements.

Methods Theoretical modeling was performed using a formalism of classical electrodynamics with the numerical

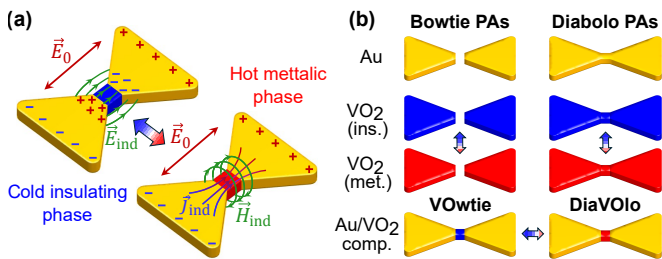


FIG. 1. (a) Bowtie and diabolo antennas with schemes of their operation and formation of hot spots. (b) Bowtie (left) and diabolo (right) antennas involved in our study: gold (first row), vanadium dioxide (second and third row), and composite (fourth row). The color of individual PA parts indicates their material composition: gold (yellow), metallic VO₂ (red), and insulating VO₂ (blue).

solution performed using the finite element method (software package Comsol Multiphysics). The geometry of the modeled PAs was set as follows: the length $L = 500$ nm, the width $W = 300$ nm, the length and the width of the bridge $B_L = 40$ nm and $B_W = 40$ nm, respectively, the thickness $T = 30$ nm. The dielectric function of gold was taken from Ref. [26] and the dielectric function of VO₂ was taken from Ref. [27].

Results The bowtie and diabolo PAs are schematically shown in Fig. 1(a). They consist of two triangular metallic wings with the proximal vertices either separated by an insulating gap (bowtie) or connected with a conducting bridge (diabolo). When excited with a plane wave polarized parallel to the long axis of the PA [as indicated by red arrows in Fig. 1(a)], the LSP resonances result in the formation of hot spots, as indicated in Fig. 1(a). In the case of the bowtie PA, the charge is concentrated on the sides of the insulating gap, resulting in the electric hot spot. In the case of the diabolo PA, the current is funnelled through the conducting bridge, resulting in the magnetic hot spot. The properties of the bowtie and diabolo PAs, their LSP resonances, and hot spots have been thoroughly studied [15, 16, 20, 21, 28, 29].

Figure 1(b) represents 8 PAs involved in our comparison. The first set consists of two gold PAs: the bowtie and the diabolo. These PAs are static; they cannot be switched. The second set consists of four VO₂ PAs: the metallic bowtie and diabolo, and the insulating bowtie and diabolo which do not support plasmon resonance. Here, switching is possible, but only between the operational (metallic) PA and the non-operational insulating structure (e.g., between the metallic VO₂ bowtie antenna supporting an electric hot spot and the insulating VO₂ bowtie structure which lacks any functionality of a PA). We refer to this switching between a certain functionality and no functionality as ON/OFF switching. Finally, the third set includes two composite PAs, the VOWtie and the diaVOlo, which can be mutually reconfigured from one to the other (and vice versa) by switching the cen-

tral VO₂ element from the insulating gap to the metallic bridge (and vice versa). In this way, a switching between the electric and the magnetic hot spot can be expected.

In the following, we compare optical properties of these 8 PAs. First, we inspect PAs of the same geometry separately (i.e., the set of 4 bowties and the set of 4 diabolos) to address the effect of the involved material system. Next, we focus on the switching, comparing VOWtie and diaVOlo, and, as a reference, also gold bowtie and diabolo (although they can only be replaced by one another, not dynamically switched). PAs are illuminated with a plane wave polarized along the long axis of PAs, as shown in Fig. 1(a).

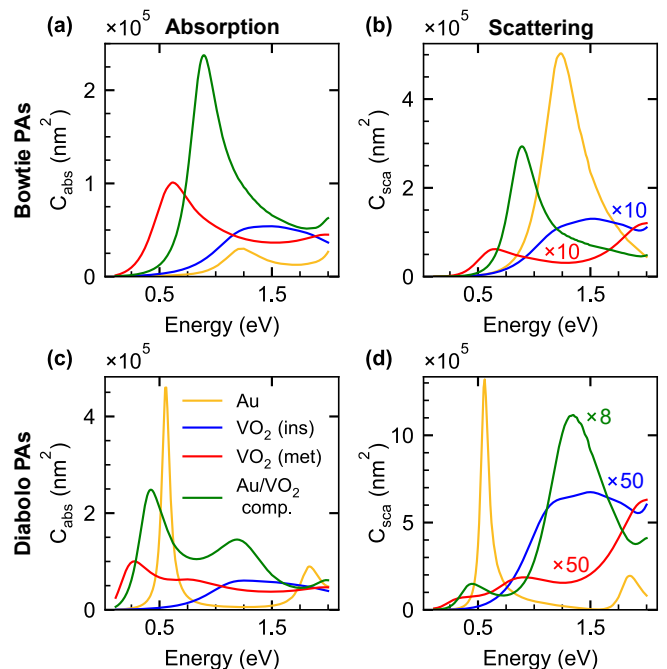


FIG. 2. Optical cross sections of bowtie and diabolo PAs. (a,b) Absorption cross section (a) and scattering cross section (b) of the bowtie PAs: gold bowtie PA (yellow line), metallic VO₂ bowtie PA (red line), insulating VO₂ bowtie structure (blue line), and composite VOWtie PA (green line). (c,d) Absorption cross section (c) and scattering cross section (d) of the diabolo PAs: gold diabolo PA (yellow line), metallic VO₂ diabolo PA (red line), insulating VO₂ diabolo structure (blue line), and composite diaVOlo PA (green line).

To identify the spectral position of the hot spots and related LSP modes, we inspect optical cross sections (the absorption and the scattering cross section), defined as the power absorbed and scattered by the PA divided by the intensity of the illumination, respectively. Fig. 2 shows the spectral dependence of both the cross sections and Tabs. I, II list several parameters relevant for the performance of PAs which were derived from the spectra of Fig. 2.

All bowtie PAs (gold, metallic VO₂, and VOWtie) exhibit a single peak in both cross sections in the spectral

TABLE I. Optical parameters of the bowtie PAs: LDB energy defined as the central position of the absorption peak (E), peak values of the normalized absorption (Q_{abs}) and scattering Q_{scat} cross section, and SAR ($Q_{\text{scat}}/Q_{\text{abs}}$).

	E (eV)	Q_{abs}	Q_{scat}	SAR
gold bowtie	1.25	0.381	6.36	16.7
VOwtie	0.890	3.02	3.73	1.24
metallic VO ₂ bowtie	0.620	1.28	0.0770	0.0604

TABLE II. Optical parameters of the diablo PA: LDB energy defined as the central position of the absorption peak (E), peak values of the normalized absorption (Q_{abs}) and scattering Q_{scat} cross section, and SAR ($Q_{\text{scat}}/Q_{\text{abs}}$).

	E (eV)	Q_{abs}	Q_{scat}	SAR
gold diablo	0.560	5.84	16.8	2.87
diaVOlo	0.420	3.16	0.229	0.0726
metallic VO ₂ diablo	0.280	1.27	0.0140	0.0112

range between 0.6–1.3 eV. This peak is assigned to the longitudinal dipole bonding (LDB) mode (as defined in Ref. [20]) responsible for the formation of the electric hot spot based on the analysis of induced fields, of which an example is shown in Fig. 3. It is customary to define normalized cross sections as cross section divided by the PA geometric cross section (i.e., the area of PA, around $8 \times 10^4 \text{ nm}^2$ in our case), and peak values of the normalized cross sections are listed in Tab. I together with the scattering to absorption ratio (SAR) defined as the peak scattering cross section divided by peak absorption cross section. They demonstrate strong plasmonic response of gold bowtie and VOwtie, with the optical cross sections reading several multiples of the PA geometric cross section, and decent plasmonic response of the metallic VO₂ bowtie. We also readily observe the distinct character of individual bowties. The gold bowtie shows a strong scattering ($5.0 \times 10^5 \text{ nm}^2$) and decent absorption ($3.0 \times 10^4 \text{ nm}^2$). The VOwtie exhibits somewhat reduced scattering (reaching 59 % of its gold-bowtie equivalent) but pronouncedly enhanced absorption ($7.9 \times$ of its gold-bowtie equivalent). Interestingly, the absorption and the scattering are nearly balanced for the VOwtie, evidenced by the near-one SAR. We stress that the pronounced difference between the gold bowtie and the VOwtie is related to a minor material modification of the gap, which represents only about 5 % of the total PA volume. However, this is not surprising, as the electric field exhibits a hot spot in the PA gap.

The metallic VO₂ bowtie is inferior to the gold bowtie and VOwtie, with considerably lower absorption cross section and negligible scattering cross section, naturally related to high optical absorption of VO₂. At the LDB energy (1.25 eV in the gold bowtie and 0.62 eV in the metallic VO₂ bowtie), the dielectric function VO₂ reads $-10.13 + i12.12$ with the intrinsic Q factor of 0.84, while

the dielectric function of gold reads $-40.30 + i1.85$ with considerably higher intrinsic Q factor of 21.8. Still, there are two findings of interest: (1) The normalized absorption cross section exceeding unity in the resonance highlights that the optical response is dominated by LSP. For comparison, a planar layer of the same material would yield a high reflection of 67 % and only a moderate absorption of 17 %. (2) Particularly low SAR of 0.0604 makes the metallic VO₂ bowtie suitable for applications in the energy harvesting or antireflection coating. For completeness, we include to our comparison also the insulating VO₂ bowtie. This structure is not plasmonically active, and exhibits only a weak absorption response above 1.2 eV related to the material absorption in VO₂.

All diablo PAs (gold, metallic VO₂, and diaVOlo) exhibit the lowest-energy peak in both cross sections in the spectral range between 0.3–0.6 eV, attributed to the longitudinal dipole (LD) mode responsible for the formation of the magnetic hot spot (see Ref. [20] for details). The assignment of the peak to the LD mode again relies on the analysis of the induced field, as exemplified in Fig. 3. The role of the material composition is mostly similar to the bowties, with the exception of the diaVOlo PA. The gold diablo PA provides efficient scattering and absorption, the metallic VO₂ diablo PA provides moderate scattering and very low SAR, and the insulating VO₂ diablo structure lacks any plasmonic response. The diaVOlo PA offers a sizeable absorption (although weaker than the gold diablo PA), but its scattering is negligible (similar to metallic VO₂ PAs and unlike the VOwtie). We attribute this to the large optical losses in the metallic VO₂ and to the fact that the absorption in the diablo bridge is significantly larger than the absorption in the bowtie gap due to a large current density in the bridge (while in the bowtie, the current is not transferred through the gap). The low SAR and the large absorption make the diaVOlo PA well suited for the same applications as the metallic VO₂ bowtie and diablo PAs (among others, the antireflection coatings), with better performance as its absorption is approximately twice as large.

In the following, we will discuss the electromagnetic field produced by the PAs (normalized by the incident plane wave) with a special focus on the hot spots. Fig. 3 shows the spatial distribution of the field for the VOwtie and diaVOlo PAs at the energy of the LDB (0.89 eV) and LD (0.42 eV) mode, respectively (i.e., at the energy of the LSP resonance supporting the corresponding hot spot). We indeed observe a formation of the electric hot spot by the VOwtie PA [Fig. 3(a)] and the magnetic hot spot by the diaVOlo PA [Fig. 3(d)] in the central part (the gap or the bridge) of PAs. Interestingly, we also observe rather unexpected localization of the remaining field components [i.e., the magnetic field of the VOwtie in Fig. 3(b) and the electric field of the diaVOlo in Fig. 3(c)] in the central part of PAs. Consequently, the hot spots

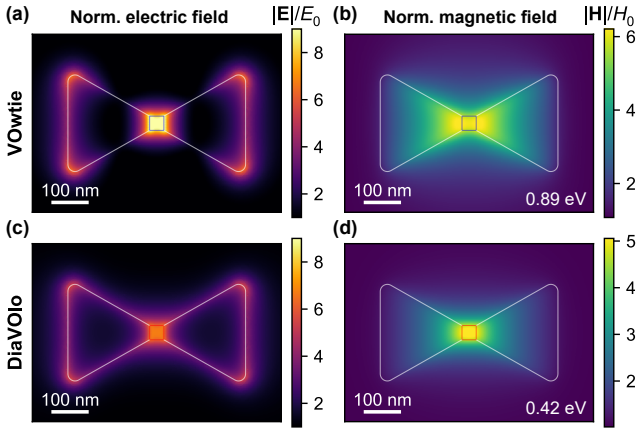


FIG. 3. Normalized electromagnetic field produced by the VOWtie and diaVOlo PAs: planar cross sections at the height of 10 nm above the upper surface of PAs. PA boundaries are indicated by the white line. (a,b) The electric (a) and the magnetic (b) field of the VOWtie PA. (c,d) The electric (c) and the magnetic (d) field of the diaVOlo PA.

supported by the VOWtie and diaVOlo PAs have strong mixed electric-magnetic character attributed to the non-zero conductivity of the gap in the VOWtie and the low conductivity (when compared to gold) of the bridge in the diaVOlo. This feature is not observed in gold or metallic VO₂ PAs, as demonstrated in Fig. 4 and Tab. III.

For a quantitative comparison of all PAs, we inspect normalized fields at the hot spot, which we represent by the point horizontally in the center of the PA and vertically at the height of 10 nm above the upper surface of the PA, where all the fields related to the hot spot (i.e., the electric field of the bowties and the magnetic field of the diabolos) are near their maximum for all PAs. The spectral dependence of the fields is shown in Fig. 4, and the peak values are listed in Tab. III. We observe a clear hierarchy of the material platforms: the gold PAs support higher fields than the composite PAs, which are still higher than fields of the metallic VO₂ PAs. To characterize the nature of the hot spot (electric, magnetic, mixed), we define the electromagnetic contrast $C_{EH} = (E - H)/(E + H)$, where E and H are the electric and magnetic field at the hot spot, respectively. The C_{EH} takes values between -1 (pure magnetic hot spot) and 1 (pure electric hot spot). The hot spots of the gold PAs are straight (the bowtie supports an electric hot spot and the diabolo supports a magnetic hot spot). A similar statement holds for the metallic VO₂ PAs, with the diabolo supporting a mixed hot spot. On the other hand, the composite PAs support mixed hot spots with a slight preference of the electric field (C_{EH} is near zero and positive), with only a minor difference between the VOWtie and the diaVOlo PAs. Their functionality thus differs from the functionality of the homogeneous bowtie and diabolo PAs, with a specific field of applications.

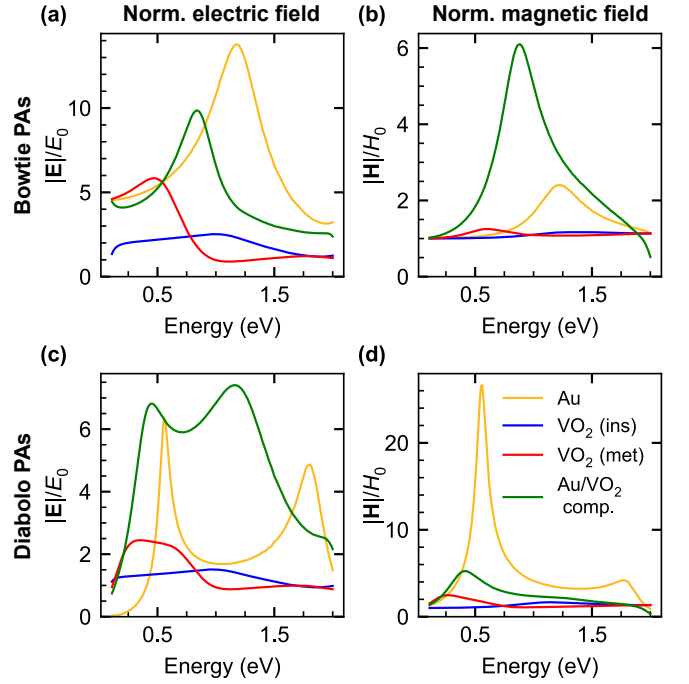


FIG. 4. Normalized electromagnetic field produced by the bowtie and diabolo PAs: Spectral dependence at the point above the center of the PA, 10 nm above the upper surface. (a,b) The electric (a) and the magnetic (b) field of the bowtie PAs. (c,d) The electric (c) and the magnetic (d) field of the diabolo PAs. The colors indicate the material composition: gold (yellow), metallic VO₂ (red), and composite (green).

TABLE III. Normalized electric (E) and magnetic (H) field and their contrast C_{EH} at the hot spot of the bowtie PAs (gold bowtie, metallic VO₂ bowtie, composite VOWtie) and the diabolo PAs (gold diabolo, metallic VO₂ diabolo, composite diaVOlo).

material	bowtie			diabolo		
	E	H	C_{EH}	E	H	C_{EH}
gold	13.8	2.40	0.703	6.32	26.7	-0.617
VO ₂	5.84	1.25	0.647	2.45	2.48	-0.00620
composite	9.86	6.10	0.235	6.82	5.25	0.130

Finally, we inspect the switching performance of the PAs. We define several switching metrics (SMs): A shift of the LSP resonance $\Delta E = E_B - E_D$ (E^B and E^D are the LSP resonance energies of the bowtie and the diabolo, respectively), a change in the electromagnetic contrast $\Delta C_{EH} = C_{EH}^B - C_{EH}^D$ (the superscripts B and D again refer to the bowtie and the diabolo PAs), and a change in the scattering-absorption contrast (SAC) $\Delta C_{SA} = C_{SA}^B - C_{SA}^D$, where the SAC defined as $\Delta C_{SA} = (Q_{scat} - Q_{abs})/(Q_{scat} + Q_{abs})$ represents a normalized analogy of SAR, and Q_{scat} , Q_{abs} are the peak values of the normalized scattering and absorption cross sections. The values of the SMs are listed in Tab. IV for the composite VOWtie and diaVOlo PAs, and for ref-

erence also for gold PAs (which, naturally, cannot be dynamically switched, but can be replaced during the fabrication of a specimen).

TABLE IV. Switching metrics: The shift of the LSP resonance energy ΔE , the change in the electromagnetic contrast ΔC_{EH} , and the change in the scattering-absorption contrast ΔC_{SA} , defined as the parameter value for the bowtie minus the parameter value for the diablo.

material	ΔE (eV)	ΔC_{EH}	ΔC_{SA}
composite	0.470	0.105	0.970
gold	0.690	1.32	0.403

A switching from the VOWtie to the diaVOlo PA (or, in the case of gold, a replacement of the bowtie with the diablo) is accompanied by the spectral red shift of the lowest LSP resonance to about half of the original value. For composite PAs, the hot spot preserves its mixed character, while for the gold PAs there is a clear transformation from the electric to the magnetic hot spot. The composite PAs also undergo a pronounced change from the balanced scattering and absorption towards pure absorption. A moderate change towards the larger absorption is also observed for gold PAs, but the scattering dominates the optical response for them both.

The unique properties of the composite PAs predestinate them for specific application fields, distinct from gold bowtie and diablo PAs. Here we discuss three prospective applications: precise plasmon-enhanced spectroscopy, switchable antireflection coatings, and plasmonic optical shutters and choppers.

Plasmon-enhanced (PE) spectroscopy exploits PAs to enhance the interaction of the probing light with the examined specimen, and has multiple flavors, including plasmon-enhanced photoluminescence [9], PE Raman spectroscopy [30], surface-enhanced infrared absorption also known by its acronym as SEIRA [31], or PE electron paramagnetic resonance [10]. The role of the PAs in PE spectroscopy is twofold. In addition to the desired enhanced light-matter coupling, often proportional to the field enhancement [16], PAs also contribute with the undesired direct light scattering and absorption, hindering quantitative analysis of the acquired spectra [10]. The PAs suitable for precise PE spectroscopy should thus provide high field enhancement while having low optical cross sections, and the composite diaVOlo PAs, and to some extent also the VOWtie PAs, fulfill these requirements well.

Antireflection coatings are an integral part of many optical elements, including lenses, optical sources and detectors, or solar cells [32]. Plasmonic antireflection coatings offer several advantages over traditional designs based on the interference, such as broadband operation and tolerance to oblique incidence [32, 33]. The composite diaVOlo PAs with their negligible scattering and relatively high peak absorption (approximately $3\times$ the

physical cross section of the PA) are well-suited for such coatings. A large area density of PAs might be needed for optimum performance of the coating, and at the same time, the near-field interaction between the neighboring PAs might be detrimental to the coating performance. These requirements can be met by randomized vertical stacking of individual PAs (realized, e.g., by dispersing the PAs in a continuous medium). Switching of SAR accompanied by the large absorption finds additional applications, e.g., as thermal emitters or bolometers [34].

Optical shutters and choppers transform continuous light waves into pulses and are involved in various approaches of optical spectroscopy. The shutters and choppers based on the switching between the absorptive diaVOlo and the semi-scattering VOWtie would offer a high switching speed and exceptional stability as no mechanical movement is required. Here we again stress the possibility to trigger the switching by the electrical or optical biasing [35, 36] on the subpicosecond scale [37], and the possibility to stabilize both states of the switch in a range of temperatures due to broad hysteresis of MIT in VO₂ [38].

Conclusion We have presented a composite material platform for plasmonic switches based on the lateral arrangement of gold and VO₂. This platform enables full functional switching, and complements homogeneous plasmonic switches based on VO₂, where only ON/OFF switching is possible (i.e., switching between the plasmonic antenna functionality and weak optical response of a dielectric). As the case study, we addressed the composite VOWtie and diaVOlo PAs, formed by two metallic wings connected with the VO₂ bridge either in its insulating or conductive states, and compared them with their metallic counterparts (both gold and metallic VO₂). The hot spots produced by the composite PAs exhibited mixed electric-magnetic character, which was only weakly altered upon switching. On the other hand, we observed a strong modification of the scattering-absorption contrast and the spectral position of the hot spots upon switching. Unique properties of the composite VOWtie and diaVOlo PAs open the prospect for uncommon applications in precise plasmon-enhanced spectroscopy, switchable antireflection coatings, or optical shutters and choppers.

The data that support the findings of this article are openly available [39].

We acknowledge support from the Ministry of Education, Youth, and Sports of the Czech Republic, projects No. CZ.02.01.01/00/22_008/0004572 (QM4ST) and LM2023051 (CzechNanoLab). RŘ was supported by Brno University of Technology (project No. CEITEC VUT-J-25-8860). JK acknowledges support from the Brno Ph.D. Talent Scholarship, funded by the Brno City Municipality. We acknowledge Petr Klenovský of Masaryk University in Brno for proposing the application as optical choppers.

-
- * rostislav.repa@vutbr.cz
† krapek@vutbr.cz
- [1] L. Novotny and N. van Hulst, *Nat. Photonics* **5**, 83 (2011).
 - [2] K. Kneipp and H. Kneipp, *Beilstein Journal of Nanotechnology* **4**, 834 (2013).
 - [3] J. Aizpurua, G. W. Bryant, L. J. Richter, F. J. García de Abajo, B. K. Kelley, and T. Mallouk, *Phys. Rev. B* **71**, 235420 (2005).
 - [4] R. Chikkaraddy, B. de Nijs, F. Benz, S. J. Barrow, O. A. Scherman, E. Rosta, A. Demetriadou, P. Fox, O. Hess, and J. J. Baumberg, *Nature* **535**, 127 (2016).
 - [5] Y. Wy, H. Jung, J. W. Hong, and S. W. Han, *Accounts of Chemical Research* **55**, 831 (2022).
 - [6] L. Nan, J. Giráldez-Martínez, A. Stefancu, L. Zhu, M. Liu, A. O. Govorov, L. V. Besteiro, and E. Cortés, *Nano Letters* **23**, 2883 (2023).
 - [7] J. Gargiulo, R. Berté, Y. Li, S. A. Maier, and E. Cortés, *Accounts of Chemical Research* **52**, 2525 (2019).
 - [8] D. Radziuk and H. Moehwald, *Phys. Chem. Chem. Phys.* **17**, 21072 (2015).
 - [9] A. Kinkhabwala, Z. Yu, S. Fan, Y. Avlasevich, K. Müllen, and W. E. Moerner, *Nat. Photonics* **3**, 654 (2009).
 - [10] L. Tesi, D. Bloos, M. Hrtoň, A. Beneš, M. Hentschel, M. Kern, A. Leavesley, R. Hillenbrand, V. Krápek, T. Šikola, and J. van Slageren, *Small Methods* **5**, 2100376 (2021).
 - [11] O. Bitton, S. N. Gupta, L. Houben, M. Kvapil, V. Krápek, T. Šikola, and G. Haran, *Nat. Commun.* **11**, 487 (2020).
 - [12] H. Pei, J. Zhang, J. Li, C. Zhao, W. Peng, J. Zhu, Y. Liu, and Y. Wei, *Physics Letters A* **570**, 131293 (2026).
 - [13] L. Khosravi Khorashad, L. V. Besteiro, Z. Wang, J. Valentine, and A. O. Govorov, *The Journal of Physical Chemistry C* **120**, 13215 (2016).
 - [14] F. Benz, M. K. Schmidt, A. Dreismann, R. Chikkaraddy, Y. Zhang, A. Demetriadou, C. Carnegie, H. Ohadi, B. de Nijs, R. Esteban, J. Aizpurua, and J. J. Baumberg, *Science* **354**, 726 (2016).
 - [15] T. Grosjean, M. Mivelle, F. I. Baida, G. W. Burr, and U. C. Fischer, *Nano Letters* **11**, 1009 (2011).
 - [16] M. Hrtoň, A. Konečná, M. Horák, T. Šikola, and V. Krápek, *Phys. Rev. Appl.* **13**, 054045 (2020).
 - [17] X. Yang, D. Su, X. Yu, P. Zeng, H. Liang, G. Zhang, B. Song, and S. Jiang, *Small* **19**, 2205659 (2023).
 - [18] E. Calandrini, A. Cerea, F. D. Angelis, R. P. Zaccaria, and A. Toma, *Nanophotonics* **8**, 45 (2019).
 - [19] Y. Chen, Y. Chen, J. Chu, and X. Xu, *ACS Photonics* **4**, 567 (2017).
 - [20] V. Krápek, A. Konečná, M. Horák, F. Ligmajer, M. Stöger-Pollach, M. Hrtoň, J. Babocký, and T. Šikola, *Nanophotonics* **9**, 623 (2020).
 - [21] L. Zhou, Q. Gan, F. J. Bartoli, and V. Dierolf, *Opt. Express* **17**, 20301 (2009).
 - [22] K. Liu, S. Lee, S. Yang, O. Delaire, and J. Wu, *Materials Today* **21**, 875 (2018).
 - [23] J. Krpenský, M. Horák, J. Kabát, J. Planer, P. Kepič, V. Krápek, and A. Konečná, *Nanoscale Adv.* **6**, 3338 (2024).
 - [24] J. Kabát, R. Řepa, J. A. Hachtel, P. Kepič, V. Krápek, A. Konečná, T. Šikola, and M. Horák, Tuning of localized surface plasmons in vanadium dioxide nanoparticles via size and insulator-metal transition (2026), arXiv:2602.00673.
 - [25] S. Cueff, J. John, Z. Zhang, J. Parra, J. Sun, R. Orobtcouk, S. Ramanathan, and P. Sanchis, *APL Photonics* **5**, 110901 (2020).
 - [26] R. L. Olmon, B. Slovick, T. W. Johnson, D. Shelton, S.-H. Oh, G. D. Boreman, and M. B. Raschke, *Phys. Rev. B* **86**, 235147 (2012).
 - [27] C. Wan, Z. Zhang, D. Woolf, C. M. Hessel, J. Rensberg, J. M. Hensley, Y. Xiao, A. Shahsafi, J. Salman, S. Richter, Y. Sun, M. M. Qazilbash, R. Schmidt-Grund, C. Ronning, S. Ramanathan, and M. A. Kats, *Annalen der Physik* **531**, 1900188 (2019).
 - [28] S. Dodson, M. Haggui, R. Bachelot, J. Plain, S. Li, and Q. Xiong, *The Journal of Physical Chemistry Letters* **4**, 496 (2013).
 - [29] B. J. Roxworthy, K. D. Ko, A. Kumar, K. H. Fung, E. K. C. Chow, G. L. Liu, N. X. Fang, and K. C. J. Toussaint, *Nano Letters* **12**, 796 (2012).
 - [30] X. Wang, S.-C. Huang, S. Hu, S. Yan, and B. Ren, *Nat. Rev. Phys.* **2**, 253 (2020).
 - [31] X. Yang, Z. Sun, T. Low, H. Hu, X. Guo, F. J. García de Abajo, P. Avouris, and Q. Dai, *Advanced Materials* **30**, 1704896 (2018).
 - [32] M. K. Hedayati, S. Fahr, C. Etrich, F. Faupel, C. Rockstuhl, and M. Elbahri, *Nanoscale* **6**, 6037 (2014).
 - [33] F. Fesharaki, A. Jooshesh, V. Bahrami-Yekta, M. Mahtab, T. Tiedje, T. E. Darcie, and R. Gordon, *ACS Photonics* **4**, 1350 (2017).
 - [34] M. A. Kats, D. Sharma, J. Lin, P. Genevet, R. Blanchard, Z. Yang, M. M. Qazilbash, D. N. Basov, S. Ramanathan, and F. Capasso, *Applied Physics Letters* **101**, 221101 (2012).
 - [35] B. Wu, A. Zimmers, H. Aubin, R. Ghosh, Y. Liu, and R. Lopez, *Phys. Rev. B* **84**, 241410 (2011).
 - [36] D. Y. Lei, K. Appavoo, F. Ligmajer, Y. Sonnefraud, R. F. Haglund, and S. A. Maier, *ACS Photonics* **2**, 1306 (2015).
 - [37] D. Wegkamp and J. Stähler, *Prog. in Surf. Sci.* **90**, 464 (2015).
 - [38] M. Horák, P. Kepič, J. Kabát, M. Hájek, F. Ligmajer, A. Konečná, T. Šikola, and V. Krápek, (2024), arXiv:2408.11972.
 - [39] R. Řepa, J. Kabát, T. Šikola, and V. Krápek, (2026), Zenodo, <http://dx.doi.org/10.5281/zenodo.18759818>.